Defect-Induced Photoluminescence Enhancement and Corresponding Transport Degradation in Individual Suspended Carbon Nanotubes

Bo Wang,[1] Lang Shen,[2] Sisi Yang,[1] Jihan Chen,[3] Juliana Echternach,[3] Rohan Dhall,[3] DaeJin Kang,[4] and Stephen Cronin[1,3]

[1]*Department of Physics and Astronomy, University of Southern California, Los Angeles, California 90089, USA*

[2]*Mork Family Department of Chemical Engineering and Material Science, University of Southern California, Los Angeles, California 90089, USA*

[3]*Ming Hsieh Department of Electrical Engineering, University of Southern California, Los Angeles, California 90089, USA*

[4]*Department of Mechatronics Engineering, Korea Polytechnic University, Siheung, Gyeonggi 15073, Republic of Korea*

(Received 16 July 2017; revised manuscript received 19 February 2018; published 16 May 2018)

This paper is a contribution to the Physical Review Applied *collection in memory of Mildred S. Dresselhaus.*

The utilization of defects in carbon nanotubes to improve their photoluminescence efficiency has become a widespread study of the realization of efficient light-emitting devices. Here, we report a detailed comparison of the defects in nanotubes (quantified by Raman spectroscopy) and photoluminescence (PL) intensity of individual suspended carbon nanotubes (CNTs). We also evaluate the impact of these defects on the electron or hole transport in the nanotubes, which is crucial for the ultimate realization of optoelectronic devices. We find that brightly luminescent nanotubes exhibit a pronounced D-band in their Raman spectra, and vice versa, dimly luminescent nanotubes exhibit almost no D-band. Here, defects are advantageous for light emission by trapping excitons, which extend their lifetimes. We quantify this behavior by plotting the PL intensity as a function of the I_D/I_G-band Raman intensity ratio, which exhibits a Lorentzian distribution peaked at $I_D/I_G = 0.17$. For CNTs with a I_D/I_G ratio >0.25, the PL intensity decreases, indicating that above some critical density, nonradiative recombination at defect sites dominates over the advantages of exciton trapping. In an attempt to fabricate optoelectronic devices based on these brightly luminescent CNTs, we transfer these suspended CNTs to platinum electrodes and find that the brightly photoluminescent nanotubes exhibit nearly infinite resistance due to these defects, while those without bright photoluminescence exhibit finite resistance. These findings indicate a potential limitation in the use of brightly luminescent CNTs for optoelectronic applications.

DOI: 10.1103/PhysRevApplied.9.054022

I. INTRODUCTION

Enhanced photoluminescence in carbon nanotubes and 2D materials due to defect-localized exciton states has been reported by several research groups over the past few years [1–11]. This work typically requires defects to be created through some form of postgrowth treatment. For example, oxygen doping of carbon nanotubes (CNTs) through ozonolysis has been shown to produce localized exciton states that exhibit enhanced photoluminescence intensities (approximately 20×), long photoluminescence lifetimes (>1 ns), and single-photon emission, even at room temperature [12–15]. These oxygen dopant sites in carbon nanotubes are well understood with a detailed atomic scale picture based on density-functional-theory calculations, and robust methods exist for creating these defect or dopant sites. UV or ozone treatment of air-suspended CNTs is also shown to provide up to fivefold enhancements in the photoluminescence (PL) intensity by the creation of such defects. While there have been many purely optical studies of CNTs, studies of optoelectronic phenomena are relatively few [16–20]. Also, a vast majority of previous carbon nanotube studies were performed on large ensembles of nanotubes rather than individual CNTs.

In the work presented here, we correlate the defect density in as-grown CNTs with their PL intensity without requiring the need for any postgrowth processing. Previous studies were carried out on ensembles of nanotubes, and, thus, it was not possible to obtain a one-to-one correlation between the PL intensity and the D-band Raman mode, which provides a relative measure of the amount of defects in carbon nanotubes [21–23]. Here, we study air-suspended CNTs rather than surfactant-suspended CNTs. The electrical resistance is used to further characterize the nature of

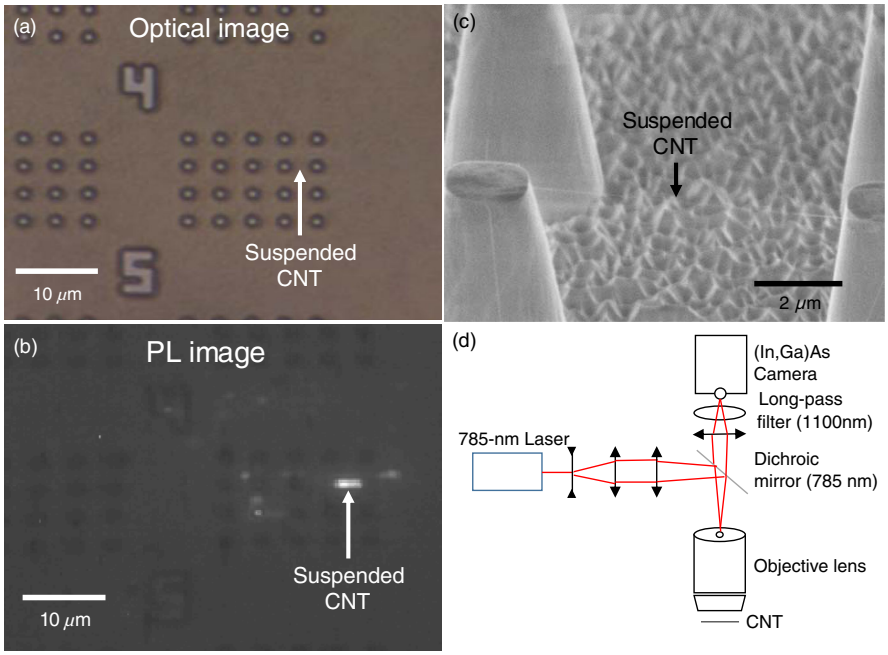

FIG. 1. (a) Optical, (b) photoluminescence, and (c) SEM images of carbon nanotubes suspended across quartz pillars. (d) Schematic diagram of the photoluminescence imaging setup.

these defects and the extent to which they perturb the electron or hole transport in this system.

II. EXPERIMENTAL SETUP AND METHOD

The samples are fabricated by etching 8-μm-deep 2×2 μm^2 pillars in a quartz substrate using a Cl-based reactive ion etch plasma. Optical and electron microscopy images of these pillars are shown in Fig. 1. Before etching, a 1-nm-thick film of Fe is deposited by electron-beam evaporation to serve as a catalyst for the nanotube growth. Carbon nanotubes are grown by chemical vapor deposition using ethanol as the carbon feedstock at 825 °C, as reported previously [24,25]. Figure 1(c) shows a scanning-electron-microscope (SEM) image of CNTs suspended across these pillars grown using this technique. The PL-related data are collected on a homebuilt PL imaging system at room temperature, as shown in Fig. 1(d). In this system, a 785-nm wavelength laser source (Spectra-Physics Model 3900) is used to irradiate the sample. The illumination area is approximately 60 μm in diameter. A 1100-nm long-pass filter is used to eliminate any Rayleigh- or Raman-scattered light. The PL signal is then collected with a thermoelectrically cooled (In,Ga)As camera (Xenics, Inc.), which is sensitive to IR light emission in the (1100–1600)-nm wavelength range. This IR camera is capable of outputting the light intensity for selected regions or individual pixels in the PL image. During these PL measurements, all the bright nanotubes of interest are moved to the same position relative to the center of the excitation area, and the PL intensity is obtained from the same pixel in order to minimize the variation between measurements. An optical microscope image of a 4×5 array of quartz pillars is shown in Fig. 1(a). Figure 1(b) shows a PL image taken from the same region of this sample. A bright line can be seen connecting two adjacent pillars corresponding to PL emission from a suspended CNT. Raman spectra from these same individual suspended

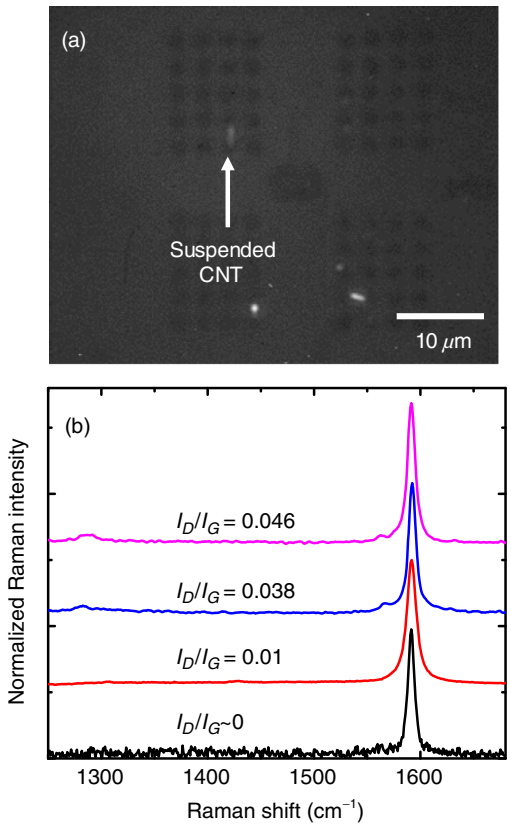

FIG. 2. (b) Raman spectra of four different suspended carbon nanotubes that exhibit dim photoluminescence and (a) representative photoluminescence image.

CNTs are collected using a Renishaw inVia microspectrometer. All Raman spectra are measured at room temperature using a 785-nm laser source with the same incident laser power, objective lens, grating, and integration time. Before collecting each Raman spectrum, several attempts are made to optimize the position and obtain the strongest Raman signal.

III. RESULTS AND DISCUSSION

Figure 2 shows the Raman spectra of four different suspended carbon nanotubes that exhibit dim photoluminescence. Figure 2(a) shows a representative photoluminescence image of one such dim nanotube. For all four nanotubes, the D-band is almost undetectable in these Raman spectra. The I_D/I_G-band Raman intensity ratio for these nanotubes spans a range from 0 to 0.041.

Figure 3 shows the Raman spectra of five brightly photoluminescent CNTs, along with a representative PL image [Fig. 3(a)]. All of these Raman spectra exhibit pronounced D-bands, indicating the presence of a substantial amount of defects in these nanotubes. Here, the I_D/I_G-band Raman intensity ratio spans a range from 0.075 to 0.16. Here, we believe that exciton localization at these defect sites prevents nonrecombination that occurs at the ends of the CNT, ultimately extending their luminescence efficiencies and lifetimes. Interestingly, even though the defect-enhanced PL is provided by localized excitons (i.e., 0D system), these nanotubes appear as lines in the PL images, indicating that there are many such defects along the length of each nanotube. The spatial resolution of our PL imaging setup is around 0.5 μm, as shown in Fig. S1 in the Supplemental Material [26].

Figure 4 shows the Raman spectra of four nanotubes that exhibit I_D/I_G-band Raman intensity ratios greater than 0.25. These highly defective nanotubes exhibit relatively dim photoluminescence. Here, we believe that nonradiative recombination at these defect sites outweighs the advantageous effects of exciton trapping created by these defect sites. It is also possible that these nanotubes have more substantial types of defects, such as vacancies or five to seven defects.

Figure 5 plots the PL intensity of 13 nanotubes as a function of the I_D/I_G-band Raman intensity ratio. Here, the data exhibit a Lorentzian distribution peaked at $I_D/I_G = 0.17$. The wide dynamic range of the PL, here spanning almost 2 orders of magnitude, is immediately apparent in this plot. For CNTs with I_D/I_G ratios <0.15, the PL intensity increases with the defect density due to

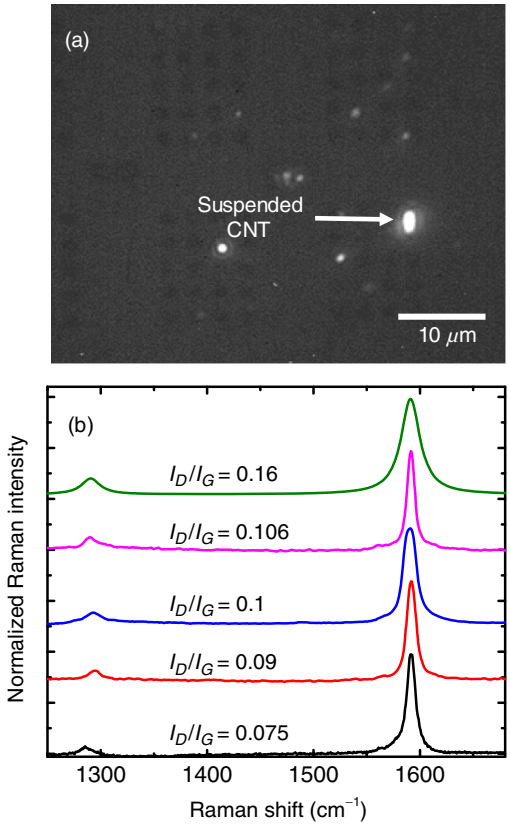

FIG. 3. (b) Raman spectra of five different suspended carbon nanotubes that exhibit bright photoluminescence and (a) representative photoluminescence image.

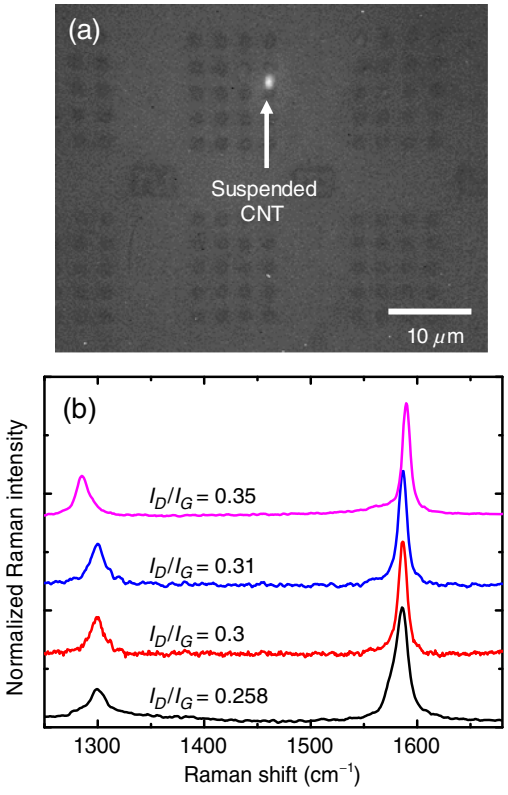

FIG. 4. (a) Representative PL image and (b) Raman spectra of four different suspended carbon nanotubes that exhibit I_D/I_G ratios >0.25.

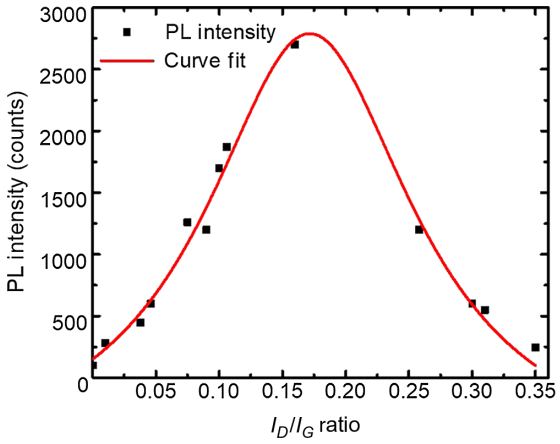

FIG. 5. Photoluminescence intensity plotted as a function of the I_D/I_G-band Raman intensity ratio for 13 different suspended carbon nanotubes. The data here are fit to a Lorentzian function centered around $I_D/I_G = 0.17$.

exciton localization. However, for CNTs with I_D/I_G ratios >0.25, the PL intensity decreases, indicating that above some critical density, nonradiative recombination at the defect sites dominates over the advantages of exciton localization.

In an attempt to fabricate optoelectronic devices based on these brightly luminescent nanotubes, we develop a flip-chip transfer process to transfer brightly photoluminescent nanotubes suspended across quartz pillars to prepatterned metal electrodes (i.e., Pt) on a separate chip, as illustrated in Fig. 6. In this process, the CNT-containing pillars are slowly brought into contact with the electrode chip using a homebuilt contact aligner. The quartz substrate is then lifted off slowly using a z-axis micromanipulator, resulting in complete transfer of the desired nanotube to the metal electrodes, suspended over the trench. Figure 6(d) shows an optical microscope image of the two chips in contact during the transport process.

Figure 7(a) shows a SEM image of a suspended CNT that is successfully transferred using this technique. Disappointingly, 11 out of 11 bright nanotubes that are successfully transferred to these electrodes show an extremely high resistance ($R > 1$ GΩ) due to the defects associated with exciton trapping. It is worth mentioning that the one-dimensional nature of CNTs makes them particularly susceptible to defects, since electrons can scatter only backwards. Figure 7(b) shows the current-gate-voltage (I-V_{gate}) characteristics of a nonbright nanotube that is transferred to these electrodes. Here, the suspended nanotube is first identified by SEM rather than PL imaging. The I-V_{gate} characteristics show field-effect transistor behavior that is typical of a semiconducting nanotube with a weak gate. Here, the effect of the underlying silicon gate is weak because the electrodes are 8 μm tall, and, hence, the underlying silicon is relatively far away from the CNT channel. Nevertheless, at a gate voltage of $V_{\text{gate}} = -4$ V, the suspended nanotube exhibits a resistance of 200 kΩ, which is at least 3 orders of magnitude lower than that of the brightly photoluminescent nanotubes that are transferred to the same electrodes. These data indicate the strong role that these defects play in preventing electron or hole transport, which will likely limit practical applications in electronically driven light emission from carbon nanotubes.

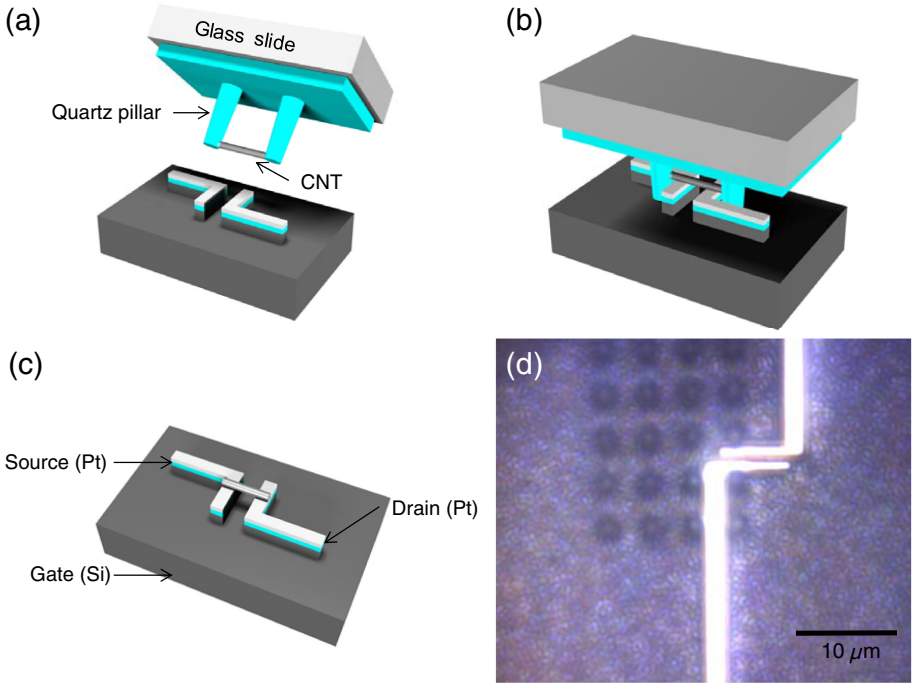

FIG. 6. (a)–(c) Schematic diagrams and (d) optical microscope image of the flip-chip transfer process.

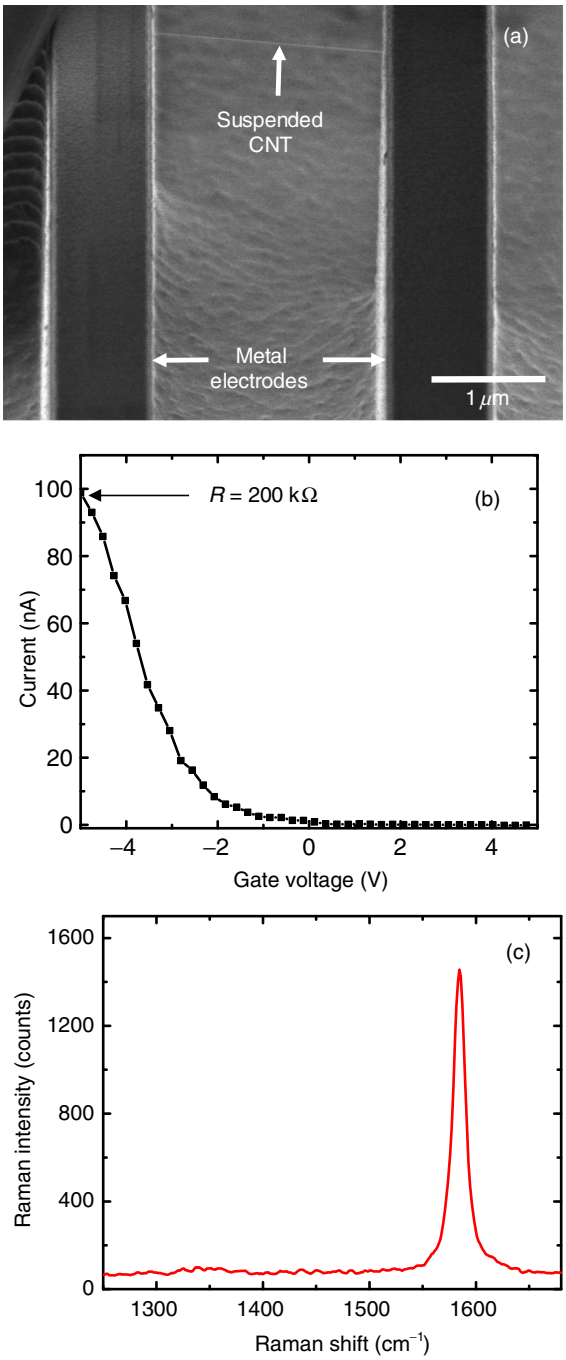

FIG. 7. (a) SEM image, (b) current-voltage characteristics, and (c) Raman spectrum of a CNT that is successfully transferred to metal electrodes.

IV. SUMMARY

In conclusion, we compare the Raman spectra and PL intensities of individual suspended CNTs. We find that brightly luminescent nanotubes exhibit pronounced D-bands in their Raman spectra, whereas dimly luminescent nanotubes exhibit almost no D-band. The relative defect density is quantified using the I_D/I_G-band Raman intensity ratio. By plotting the PL intensity as a function of the I_D/I_G-band Raman intensity ratio, we observe a Lorentzian distribution peaked at $I_D/I_G = 0.17$. CNTs with a I_D/I_G ratio above 0.25 show a decreased PL intensity, indicating the point beyond which defects cause nonradiative recombination rather than exciton trapping. When these brightly luminescent nanotubes are transferred to metal electrodes, their resistance is found to be infinite ($R > 1$ GΩ) because of the presence of these defects. However, nonluminescent CNTs exhibit finite resistance. These results indicate that there may be an inherent limitation in the ultimate realization of optoelectronic devices with a trade-off between luminescence efficiency and low-resistance carrier transport.

The spatial resolution of our PL imaging setup is around 1 μm, and the resistance of a blank chip used in the flip-chip transfer technique is around 2 GΩ, as shown in the Supplemental Material [26].

ACKNOWLEDGMENTS

The authors would like to acknowledge support from the Northrop Grumman Institute of Optical Nanomaterials and Nanophotonics (B. W). This research is also supported by the Department of Energy Award No. DE-FG02-07ER46376 (J. C.) and National Science Foundation Grant No. 1402906 (S. Y.). A portion of this work is carried out in the University of California Santa Barbara nanofabrication facility.

[1] Y. M. Piao, B. Meany, L. R. Powell, N. Valley, H. Kwon, G. C. Schatz, and Y. H. Wang, Brightening of carbon nanotube photoluminescence through the incorporation of $sp(3)$ defects, Nat. Chem. **5**, 840 (2013).

[2] M. S. Hofmann, J. T. Gluckert, J. Noe, C. Bourjau, R. Dehmel, and A. Hogele, Bright long-lived and coherent excitons in carbon nanotube quantum dots, Nat. Nanotechnol. **8**, 502 (2013).

[3] I. Sarpkaya, Z. Y. Zhang, W. Walden-Newman, X. S. Wang, J. Hone, C. W. Wong, and S. Strauf, Prolonged spontaneous emission and dephasing of localized excitons in air-bridged carbon nanotubes, Nat. Commun. **4**, 2152 (2013).

[4] F. Vialla, Y. Chassagneux, R. Ferreira, C. Roquelet, C. Diederichs, G. Cassabois, P. Roussignol, J. S. Lauret, and C. Voisin, Unifying the Low-Temperature Photoluminescence Spectra of Carbon Nanotubes: The Role of Acoustic Phonon Confinement, Phys. Rev. Lett. **113**, 057402 (2014).

[5] H. Y. Nan, Z. L. Wang, W. H. Wang, Z. Liang, Y. Lu, Q. Chen, D. W. He, P. H. Tan, F. Miao, X. R. Wang, J. L. Wang, and Z. H. Ni, Strong photoluminescence enhancement of MoS_2 through defect engineering and oxygen bonding, ACS Nano **8**, 5738 (2014).

[6] S. Tongay, J. Suh, C. Ataca, W. Fan, A. Luce, J. S. Kang, J. Liu, C. Ko, R. Raghunathanan, J. Zhou, F. Ogletree, J. B. Li, J. C. Grossman, and J. Q. Wu, Defects activated photoluminescence in two-dimensional semiconductors: Interplay

between bound, charged, and free excitons, Sci. Rep. **3**, 2657 (2013).

[7] H. Harutyunyan, T. Gokus, A. A. Green, M. C. Hersam, M. Allegrini, and A. Hartschuh, Defect-induced photoluminescence from dark excitonic states in individual single-walled carbon nanotubes, Nano Lett. **9**, 2010 (2009).

[8] Y. M. He, G. Clark, J. R. Schaibley, Y. He, M. C. Chen, Y. J. Wei, X. Ding, Q. Zhang, W. Yao, X. D. Xu, C. Y. Lu, and J. W. Pan, Single quantum emitters in monolayer semiconductors, Nat. Nanotechnol. **10**, 497 (2015).

[9] C. Chakraborty, L. Kinnischtzke, K. M. Goodfellow, R. Beams, and A. N. Vamivakas, Voltage-controlled quantum light from an atomically thin semiconductor, Nat. Nanotechnol. **10**, 507 (2015).

[10] A. Srivastava, M. Sidler, A. V. Allain, D. S. Lembke, A. Kis, and A. Imamoglu, Optically active quantum dots in monolayer WSe_2, Nat. Nanotechnol. **10**, 491 (2015).

[11] M. Koperski, K. Nogajewski, A. Arora, V. Cherkez, P. Mallet, J. Y. Veuillen, J. Marcus, P. Kossacki, and M. Potemski, Single photon emitters in exfoliated WSe_2 Structures, Nat. Nanotechnol. **10**, 503 (2015).

[12] X. Ma, L. Adamska, H. Yamaguchi, S. E. Yalcin, S. Tretiak, S. K. Doorn, and H. Htoon, Electronic structure, and chemical nature of oxygen dopant states in carbon nanotubes, ACS Nano **8**, 10782 (2014).

[13] S. Ghosh, S. M. Bachilo, R. A. Simonette, K. M. Beckingham, and R. B. Weisman, Oxygen doping modifies near-infrared band gaps in fluorescent single-walled carbon nanotubes, Science **330**, 1656 (2010).

[14] Y. Miyauchi, M. Iwamura, S. Mouri, T. Kawazoe, M. Ohtsu, and K. Matsuda, Brightening of excitons in carbon nanotubes on dimensionality modification, Nat. Photonics **7**, 715 (2013).

[15] X. D. Ma, N. F. Hartmann, J. K. S. Baldwin, S. K. Doorn, and H. Htoon, Room-temperature single-photon generation from solitary dopants of carbon nanotubes, Nat. Nanotechnol. **10**, 671 (2015).

[16] J. Chen, V. Perebeinos, M. Freitag, J. Tsang, Q. Fu, J. Liu, and P. Avouris, Bright infrared emission from electrically induced excitons in carbon nanotubes, Science **310**, 1171 (2005).

[17] E. Adam, C. M. Aguirre, L. Marty, B. C. St-Antoine, F. Meunier, P. Desjardins, D. Menard, and R. Martel, Electroluminescence from single-wall carbon nanotube network transistors, Nano Lett. **8**, 2351 (2008).

[18] M. Freitag, V. Perebeinos, J. Chen, A. Stein, J. C. Tsang, J. A. Misewich, R. Martel, and P. Avouris, Hot carrier electroluminescence from a single carbon nanotube, Nano Lett. **4**, 1063 (2004).

[19] S. Khasminskaya, F. Pyatkov, K. Slowik, S. Ferrari, O. Kahl, V. Kovalyuk, P. Rath, A. Vetter, F. Hennrich, M. M. Kappes, G. Gol'tsman, A. Korneev, C. Rockstuhl, R. Krupke, and W. H. P. Pernice, Fully integrated quantum photonic circuit with an electrically driven light source, Nat. Photonics **10**, 727 (2016).

[20] L. Marty, E. Adam, L. Albert, R. Doyon, D. Menard, and R. Martel, Exciton Formation and Annihilation during 1D Impact Excitation of Carbon Nanotubes, Phys. Rev. Lett. **96**, 136803 (2006).

[21] M. S. Dresselhaus, A. Jorio, A. G. Souza, and R. Saito, Defect characterization in graphene and carbon nanotubes using Raman spectroscopy, Phil. Trans. R. Soc. A **368**, 5355 (2010).

[22] M. S. Dresselhaus, G. Dresselhaus, R. Saito, and A. Jorio, Raman spectroscopy of carbon nanotubes, Phys. Rep. **409**, 47 (2005).

[23] C. C. Chang, C. C. Chen, W. H. Hung, I. K. Hsu, M. A. Pimenta, and S. B. Cronin, Strain-induced *D* band observed in carbon nanotubes, Nano Res. **5**, 854 (2012).

[24] M. R. Amer, S. W. Chang, and S. B. Cronin, Competing photocurrent mechanisms in quasi-metallic carbon nanotube *pn* devices, Small **11**, 3119 (2015).

[25] S. W. Chang, J. Theiss, J. Hazra, M. Aykol, R. Kapadia, and S. B. Cronin, Photocurrent spectroscopy of exciton and free particle optical transitions in suspended carbon nanotube *pn*-junctions, Appl. Phys. Lett. **107**, 053107 (2015).

[26] See Supplemental Material at http://link.aps.org/supplemental/10.1103/PhysRevApplied.9.054022 for the spatial profile of the electroluminescence intensity and the plot of current vs bias voltage from a blank chip.